



Cite this: DOI: 10.1039/c5ib00206k

## Assessment of the potential of a high frequency acoustomicrofluidic nebulisation platform for inhaled stem cell therapy†

Layla Alhasan,<sup>abc</sup> Aisha Qi,<sup>b</sup> Amgad R. Rezk,<sup>b</sup> Leslie Y. Yeo<sup>b</sup> and Peggy P. Y. Chan<sup>\*bd</sup>

Despite the promise of stem cell therapy for lung therapeutics and repair, there are few viable means for directly delivering stem cells to locally target the respiratory airways *via* inhalation. This is not surprising given the significant challenges in aerosolising stem cells, particularly given their susceptibility to damage under the large stresses involved in the nebulisation process. Here, we present promising results using a microfluidic acoustic nebulisation platform that is not only low cost and portable, but also its high MHz order frequencies are effective for preserving the structural and functional integrity of mesenchymal stem cells (MSCs) during the nebulisation process. This is verified through an assessment of the viability, structure, metabolic activity, proliferation ability and genetic makeup of the nebulised MSCs using a variety of assays, including cell viability staining, flow cytometry, reverse transcription and quantitative polymerase chain reaction, and immunophenotyping, thus demonstrating the platform as a promising method for efficient pulmonary stem cell delivery.

Received 14th August 2015,  
Accepted 12th November 2015

DOI: 10.1039/c5ib00206k

www.rsc.org/ibiology

### Insight, innovation, integration

Despite the promise of stem cell therapy for lung therapeutics and repair, there are few viable means for directly delivering stem cells to locally target the respiratory airways *via* inhalation. This is not surprising given the significant challenges in aerosolising stem cells, particularly given their susceptibility to damage under the large stresses involved in the nebulisation process. Here, we present promising results using a microfluidic acoustic nebulisation platform, that is not only low cost and portable, but also its high MHz order frequencies are effective for preserving the structural and functional integrity of mesenchymal stem cells (MSCs) during the nebulisation process. This is verified through biological assessments, thus demonstrating the platform as a promising method for efficient pulmonary stem cell delivery.

## Introduction

There is growing evidence that demonstrates the efficacy of stem cell based therapies for the treatment of a variety of lung diseases including chronic obstructive pulmonary disease (COPD), pulmonary and cystic fibrosis, and pulmonary hypertension.<sup>1,2</sup> This is especially timely given the recognition of the urgency for new approaches to treat lung diseases in light of their increasing prevalence, in particular, COPD, which is anticipated to be among the top leading causes of global mortality in the next 5 years. Motivated by the shortage in donor lungs and the extremely high mortality rate (almost 50%) following

lung transplantation, there are additionally an increasing number of studies examining the potential of stem cell administration to injured lungs, from the viewpoint of both an immunomodulatory role in attenuating inflammation as well as a regenerative role in injury repair.<sup>3</sup>

There are however far fewer studies on the development of methods to administer stem cells to the lungs. While there have been investigations to show the recruitment of the cells to the lungs following systemic (*e.g.*, intravenous) administration, these depend critically on many factors.<sup>4</sup> Direct lung delivery *via* aerosol inhalation, on the other hand, not only facilitates local targeting of the disease- or injury-specific region, but also allows easy and painless administration, involves fewer side effects and avoids the need for anaesthesia.

Nevertheless, there remain considerable challenges associated with stem cell aerosolisation, in particular the likelihood that the stem cells would survive and retain their function during the nebulisation process. Their fragility therefore rules out the use of a wide number of commonly used nebulisation

<sup>a</sup> Department of Biotechnology & Biological Science, RMIT University, Melbourne, Australia

<sup>b</sup> Micro/Nanophysics Research Laboratory, RMIT University, Melbourne, Australia

<sup>c</sup> Department of Biology, Education Faculty, Thi-Qar University, Thi-Qar, Iraq

<sup>d</sup> Department of Biomedical Engineering, Swinburne University of Technology, Hawthorn, Australia. E-mail: pchan@swin.edu.au; Tel: +61 3 9214 8276

† Electronic supplementary information (ESI) available. See DOI: 10.1039/c5ib00206k

techniques, particularly those that subject the aerosols to intense stresses (*e.g.*, shear, cavitation and heat) such as jet (compressed air) and conventional ultrasonic nebulisers.<sup>5–7</sup> In contrast, electrohydrodynamic atomisation has been shown to be a viable method for stem cell delivery,<sup>8–11</sup> although the necessity for large (kV) DC potentials typically renders the electrospray impractical as a portable consumer inhalation device from a safety viewpoint.

In this work, we demonstrate the use of a novel high frequency acoustic nebulisation platform as an effective aerosolisation technique for inhaled mesenchymal stem cell (MSC) therapy. This is the first study that investigates the viability of stem cells under SAW nebulisation. These surface acoustic waves (SAWs)<sup>12,13</sup> operate at sufficiently high frequencies (10–100 MHz order)<sup>14</sup> in comparison to conventional bulk ultrasonic nebulisers (10 kHz to 1 MHz)<sup>15</sup> such that the vibrational excitation that the therapeutic molecules or cells to be nebulised are subjected to occurs over a much shorter period compared to their hydrodynamic shear relaxation time scales, thus eliminating the risk of macromolecular denaturation or cell lysis.<sup>16,17</sup> Additionally, the low powers (on the order of 1 W), which are one to two orders of magnitude less than those required by conventional ultrasonic nebulisers, not only eliminate the possibility of cavitation but also allow the possibility for miniaturised operation using a battery-powered portable handheld device.<sup>18</sup> While the efficacy of the SAW nebulisation has been demonstrated for proteins (*e.g.*, monoclonal antibodies for lung tumour inhibition<sup>19</sup>) and nucleic acids (*e.g.*, plasmid DNA for influenza vaccination<sup>20</sup>), as well as for microfluidic mass spectrometry interfacing<sup>21–23</sup> and protein substrate patterning,<sup>24</sup> there is yet to be a demonstration of the efficacy of the SAW nebulisation platform for pulmonary stem cell delivery. We note that stem cells have been shown in a previous study to retain their viability and functionality under SAW excitation, but the intensity of the vibration that the cells were subjected to in that study (typically 100 mW order) was far below the critical levels required for nebulisation.<sup>25</sup>

## Materials and methods

### Materials

Dulbecco's Modified Eagle Medium (D-MEM) low glucose, GlutaMAX™ supplement, MSC qualified fetal bovine serum (FBS), gentamycin reagent solution, Dulbecco's phosphate-buffered saline (DPBS) without Ca<sup>2+</sup> and Mg<sup>2+</sup>, TrypLE™ select enzyme, DNA-free™ kit, AlamarBlue® cell viability reagent, Quanti-iT™ PicoGreen® dsDNA assay kit, Calcein AM, propidium iodide (PI) and NP40 cell lysis buffer were purchased from Life Technologies Pty. Ltd (Mulgrave, VIC, Australia). Unless otherwise stated, all other chemicals were obtained from Sigma-Aldrich Pty. Ltd (Castle Hill, NSW, Australia).

### Cell culture

GIBCO® rat MSCs from the bone marrow of Sprague Dawley rats (Life Technologies, Mulgrave, VIC, Australia) were maintained

in cell culture medium comprising D-MEM with GlutaMAX™ supplemented with 10% MSC qualified FBS and 5 μg ml<sup>-1</sup> of gentamycin reagent solution at 37 °C in a humidified 5% CO<sub>2</sub> incubator. Cells were rinsed with DPBS followed by trypsinisation with TrypLE™ after reaching 80% confluence. The harvested cells were rinsed with cell culture medium and reconstituted to a cell suspension solution containing 2 × 10<sup>6</sup> cells per ml.

### SAW nebuliser device fabrication and setup

A 0.5 mm thick 127.68° Y-axis rotated, X-axis propagating lithium niobate wafer (Roditi Ltd, London, UK), which constituted the piezoelectric substrate on which the SAWs are generated, was first cleaned according to standard procedures.<sup>26</sup> The electrodes were then fabricated on the wafer using standard UV photolithography according to a protocol modified from Qi *et al.*<sup>27</sup> In brief, the clean wafer was sputtered with a 5 nm layer of chromium followed by a 1.5 μm layer comprising 99% aluminium and 1% copper using an electron beam evaporator (Nanochrome II, Intlvac Corp., Niagara Falls, NY, USA). The wafer was then spun-coated with a thin layer (approximately 3 μm) of AZ1512 photoresist (Microchemicals GmbH, Ulm, Germany) followed by exposure to UV through a glass mask. The next step comprised the development of the photoresist layer and wet etching using an aluminium etchant ANPE 5-5-80-10 (Microchemicals GmbH, Ulm, Germany) to generate the interdigital transducer (IDT) electrode patterns, which, in this case, consisted of elliptical single-phase unidirectional transducers (SPUDTs)<sup>28</sup> with an electrode finger width and spacing corresponding to a resonant frequency of approximately 30 MHz. The wafer containing the SPUDT was subsequently diced into microchips each with approximately 18 mm length and 12 mm width. A two-dimensional spatial distribution of the surface displacement amplitude near the focal point of the elliptical SPUDT was measured using a laser Doppler vibrometer (LDV) (UHF-120, Polytec GmbH, Waldbronn, Germany) and is shown in Fig. 1a; an in-depth investigation of the surface displacement patterns produced by various IDT designs can be found in the study of Shilton *et al.*<sup>28</sup>

To affect the nebulisation process in order to generate the aerosol-laden MSCs, the edge of a SAW microchip was partially immersed into the MSC suspension contained in a Petri dish, as depicted in Fig. 2. Rayleigh SAWs were then generated by applying an input oscillating electrical signal to the SPUDT at the resonant frequency using a signal generator (SML01, Rhode & Schwarz, Munich, Germany) and amplifier (10W1000C, Amplifier Research, Souderton, PA, USA). Above, a critical power of 1.5 W, nebulisation ensued and the resultant aerosol mist containing the MSCs was collected for further characterisation.

### Aerosol characterisation

We first characterised the SAW device to determine its nebulisation rate and the aerosol sizes under ambient conditions. The nebulisation flow rate of the SAW nebuliser device was first tuned by adjusting the input power (1.5–3 W) and the time for a fixed volume of solution to completely nebulise was

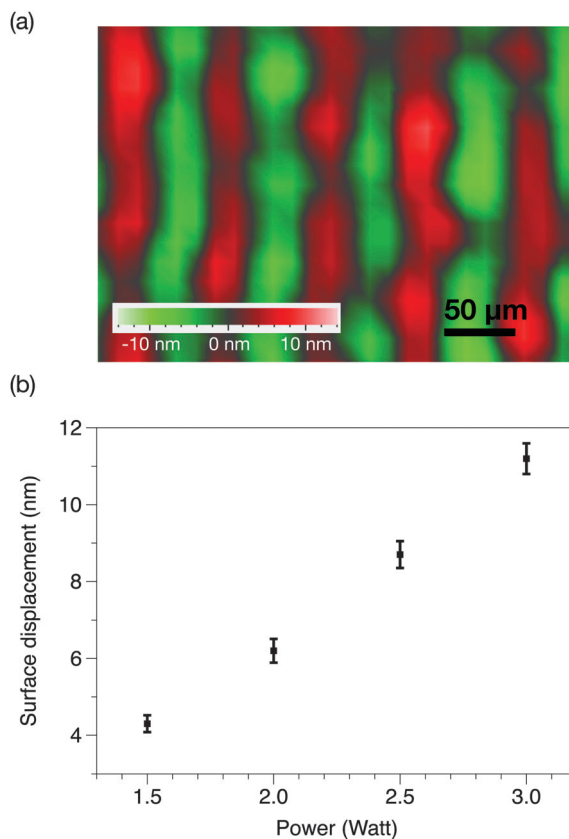


**Fig. 1** (a) Representative two-dimensional spatial distribution of the surface displacement in the focal region of the SPUDT, obtained using laser Doppler vibrometry at an input power of 2.5 W. (b) Average surface displacement as a function of the input power to the device that corresponds to the nebulisation rates tabulated in Table 1.

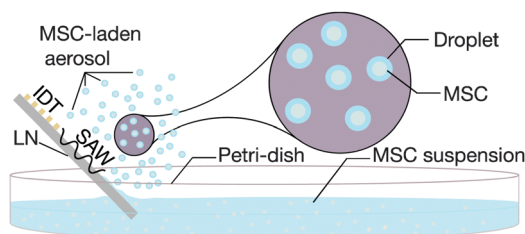


**Fig. 2** Schematic depiction of the SAW nebulisation setup for rapid aerosolisation of MSCs (not to scale). Power is supplied in the form of an oscillating electrical signal to the SPUDT electrodes photolithographically patterned onto a lithium niobate substrate. This causes the generation of a SAW, which when brought into contact with the MSC suspension in the Petri dish, nebulises the fluid to form an aerosol mist, each droplet of which is laden with the MSCs.

subsequently measured. Aerosol droplet sizes were determined using laser diffraction (Spraytec, Malvern Instruments, Malvern, UK), specified as a median diameter from a volume-based size distribution; a mean value across 5 replicates was reported.

### Characterisation of the cell morphology, viability and proliferation

For preliminary testing, the nebulised MSCs were first collected and stained with Trypan blue. Cell counting was performed

immediately to quantify the stained and unstained cells using an automated cell counter (Countess<sup>®</sup>, Life Technologies Pty. Ltd, Mulgrave, VIC Australia).

The nebulised MSCs were then transferred to a new tissue culture well-plate at a seeding density of  $5 \times 10^3$  cells per ml for re-culturing at 2 and 24 h post-nebulisation in order to determine their viability, metabolic activity and proliferation ability. The morphology of the cells was monitored using phase contrast microscopy and images were captured at various time points. The viability of the re-cultured MSCs was examined by staining the cells with Calcein AM and PI according to the manufacturer's instructions. The stained MSCs that were re-cultured for 2 h were visualised using laser scanning confocal microscopy (LSCM; Eclipse Ti, Nikon Instruments Inc., Melville, NY, USA) without further rinsing. The stained MSCs that were re-cultured for 24 h were rinsed using phosphate buffered saline (PBS) before LSCM visualisation.

For quantification, MSCs were nebulised as described above and were collected in a separate experiment. Some of these MSCs were immediately stained with Calcein AM and PI according to the manufacturer's instructions. The rest of the MSCs were transferred to a new tissue culture well-plate at a seeding density of  $5 \times 10^3$  cells per ml for re-culturing for 24 h. The re-cultured cells were then trypsinised and stained with Calcein AM and PI. Both sets of stained cells were analysed using flow cytometry (FACSCanto<sup>™</sup> II, BD Biosciences, North Ryde, NSW, Australia). As a positive control, MSCs were treated with 0.1% Triton X-100 for 2–3 min prior to staining.

The metabolic activity of the re-cultured MSCs was quantified using an AlamarBlue<sup>®</sup> assay according to Hoo *et al.*<sup>29</sup> In brief, spent medium was removed from each well prior to rinsing with DPBS. AlamarBlue<sup>®</sup> dye (10%) diluted with cell culture medium was then added into each well and incubated at 37 °C in humidified 5% CO<sub>2</sub> for 4 h. Fluorescence analysis was performed using a multi-mode microplate reader with an excitation wavelength of 570 nm and an emission wavelength of 600 nm (SpectraMax<sup>®</sup> Paradigm, Molecular Devices LLC, Sunnyvale, CA, USA).

The proliferation ability of the nebulised MSCs was determined by quantifying the deoxyribonucleic acid (DNA) content using a Picogreen<sup>®</sup> assay according to the study of Hoo *et al.*<sup>29</sup> In brief, the MSCs were trypsinised after re-culturing for 1, 3, 5 and 7 days. The cells were then twice washed using cold DPBS followed by centrifugation for 5 min at 1200 rpm. The resultant cell pellet was subsequently collected for lysis using a NP40 cell lysis buffer for 30 min on ice and vortexed every 10 min; the cell lysates were subjected to a freeze-thaw cycle prior to centrifugation at 13 000 rpm for 10 min at 4 °C. Each 100 μl of clear lysate was aliquoted in a new 96-well plate and incubated for 5 min with 100 μl of the PicoGreen<sup>®</sup> reagent. Fluorescence analysis was subsequently performed using a multi-mode microplate reader at an excitation wavelength of 480 nm and an emission wavelength of 520 nm. The number of cells in each sample was determined by correlating the DNA content with a standard curve, obtained using cell lysates containing a known number of MSCs. Non-nebulised cells were used as control for all of the above experiments.

Table 1 PCR primer sequences

Gene	Forward/reverse (5' 3')	Ref.
ITGB (CD29 protein)	AATGGAGTGAATGGGACAGG/ TCTGTGAAGCCAGAGGTTT	31
CD44	TTGGCATCCCTCCTGGCGCTGG/ AAGGAGGAAGTGAAGAGACCC	32
CD106	CCTCACTTGCAGCACTACGGGCT/ TTTCCAATATCCTCAATGACGGG-	33
GAPDH	CAAGGTCATCCATGACAACTTTG/ GTCCACCACCCTGTTGCTGTAG	34

### Reverse-transcription polymerase chain reaction (RT-PCR) and real-time polymerase chain reaction (qPCR)

The gene expression of nebulised MSCs and control MSCs was qualitatively determined using RT-PCR and quantitatively using qPCR with CD29, CD44, and CD106 as markers. Ribonucleic acid (RNA) was isolated from the MSCs using an RNAeasy mini kit (Qiagen, Chadstone, VIC, Australia) according to the manufacturer's instructions. The RNA quality and concentration were examined using a spectrophotometer (ND-1000, NanoDrop Technologies, Thermo Fisher Scientific Inc., Waltham, MA, USA). To eliminate any contaminating genomic DNA, the isolated RNA was treated with DNA-free™ kit according to the manufacturer's protocol as supplied. Complementary DNA (cDNA) generated using a QuantiTect Reverse Transcription kit (Qiagen, Chadstone, VIC, Australia) as per the manufacturer's instructions was subjected to PCR amplification using primers obtained from Geneworks Pty. Ltd (Thebarton, SA, Australia); the primer sequences are listed in Table 1. Glyceraldehyde-3-phosphate dehydrogenase (GAPDH) was used as the housekeeping gene. For RT-PCR, the PCR products were size fractionated using 1.5% agarose gel electrophoresis.

The qPCR analysis was performed using a Rotor-Gene Q (Qiagen, Chadstone, VIC, Australia) and a QuantiTect SYBR® Green PCR kit (Qiagen, Chadstone, VIC, Australia). After 10 min of denaturation at 95 °C, 40 PCR cycles were carried out at 95 °C for 15 s, 60 °C for 30 s, and 72 °C for 15 s. The relative mRNA levels were calculated using the  $\Delta\Delta C_T$  method according to the study of Sarvi *et al.*<sup>30</sup> The results were reported as fold change values compared to the non-nebulised cells.

### Immunophenotyping

MSCs were nebulised as described previously and collected for further cultivation. After 24 h of cultivation, the cells were harvested and aliquoted at a concentration of  $1 \times 10^6$  cells per sample. The cells were then washed with PBS and centrifuged at 1500 rpm three times and subsequently resuspended in buffer (0.1% bovine serum albumin (BSA) in PBS) containing antibodies and incubated on ice for 25–30 min. The MSCs were labelled with either the Alexa Fluor 488® conjugated integrin beta-1/CD29 antibody (Life Technologies, Mulgrave, VIC, Australia), FITC conjugated anti-CD44 antibody (Merck Millipore, Bayswater, VIC, Australia), or PE mouse conjugated anti-rat CD106 antibody (BioLegend, San Diego, CA, USA), followed by labelling with FITC conjugated goat anti-mouse IgG secondary antibodies (Merck Millipore, Mulgrave, VIC, Australia); the antibodies were

diluted according to the manufacturer's protocols. The labelled MSCs were then washed twice in buffer (3% BSA in PBS), followed by resuspension in 500  $\mu$ l of buffer (3% BSA in PBS) and flow cytometry analysis. 10 000 events were acquired from each sample, and the results were plotted using flow cytometry data analysis software (Flowing Software, v2.5.1, www.flowingsoftware.com). The surface marker expression of the nebulised cells was compared to that of the non-nebulised cells (control).

### Statistical analysis

All experiments were performed with at least 3 replicates. Unless otherwise stated, the results were reported as the average value  $\pm$  standard deviation. Multiple groups of data were compared using one-way analysis of variance (ANOVA), while two groups of data were compared using Student's *t*-test; data are considered statistically significant when  $p < 0.05$ .

## Results and discussion

### Aerosol characterisation

As shown in Fig. 3, the applied SAW power has a direct influence on the nebulisation rate, which increased as the applied power is ramped to approximately 350  $\mu$ l  $\text{min}^{-1}$  at 3 W ( $p < 0.0001$ ,  $n = 3$ ); the corresponding surface displacement amplitude of the SAW is plotted in Fig. 1b in which we observe a linear response in the magnitude of the surface displacement with an increase in the power input, indicating that the device has not reached its power saturation limit. In any case, these observations are consistent with previous findings on the effect of SAW irradiation on the nebulisation flow rate, given that more acoustic energy is transmitted into the fluid to drive both streaming and the destabilisation of its interface, which, in turn, leads to its breakage into aerosol droplets that constitute the nebulised mist.<sup>18</sup>

Table 2 on the other hand shows the median droplet size of the aerosols containing the MSCs for various input powers to the device. We observe the median aerosol size across all input powers to be just slightly above 13  $\mu$ m, which is similar to the size of a single MSC, thus indicating that most of the droplets contained a single cell. Given that aerosols with sizes  $> 5 \mu$ m are expected to deposit due to inertial impaction in the upper

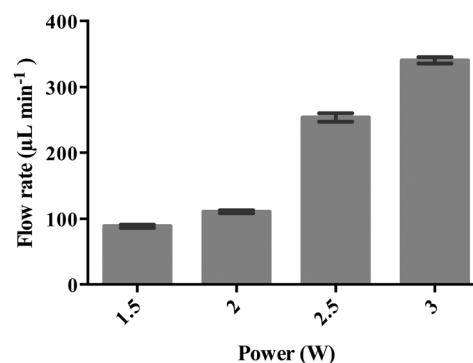


Fig. 3 SAW nebulisation rate ( $\mu\text{L min}^{-1}$ ) as a function of the applied power to the device. The data are represented in terms of a mean value ( $n = 3$ )  $\pm$  standard error.

**Table 2** Median aerosol drop size as a function of the input power to the SAW device measured using laser diffraction

Applied power (W)	Median droplet size ( $\mu\text{m}$ )
1.5	$13.17 \pm 0.29$
2.0	$13.33 \pm 0.29$
2.5	$13.50 \pm 0.50$
3.0	$13.50 \pm 0.50$

respiratory tract,<sup>35,36</sup> we envisage the potential use of the SAW device for inhaled stem cell delivery for tissue repair and regeneration within the extrathoracic (pharyngeal and laryngeal) regions.

### Cell morphology and viability

We subsequently conducted a preliminary study to optimise the SAW nebulisation in terms of maximising retention of the cell viability post-nebulisation. Here, the cells were examined using the Trypan blue assay immediately after being nebulised and the cell viability calculated by normalising the number of viable cells in the nebulised samples against the number of viable cells in the untreated samples. As shown by the data in Fig. 4, the number of viable cells decreases with increasing applied power, possibly due to the increase in the stresses that the cells are subjected to with increasing levels of acoustic radiation pressure. This observation is consistent with a previous study on using SAW radiation to drive osteoblast perfusion into tissue scaffolds (although not *via* nebulisation), in which the cell viability was found to decrease with increasing applied power.<sup>37</sup> Nevertheless, it is encouraging to note that the cell viability normalised by that of the control cells remains relatively high—close to 90% even at 1.5 W, which, together with the  $100 \mu\text{l min}^{-1}$  delivery at this power (Fig. 3), adequate for most stem cell therapeutic applications, demonstrates the potential efficacy of the device as a platform for pulmonary stem cell delivery.

To minimise the loss in stem cell viability, the device was henceforth operated at the optimum applied power of 1.5 W. Fig. 5 shows representative LSCM images of the cells stained with Calcein AM and PI after being seeded on a new well-plate and allowed to cultivate for 2 and 24 h. At 2 h post-nebulisation,

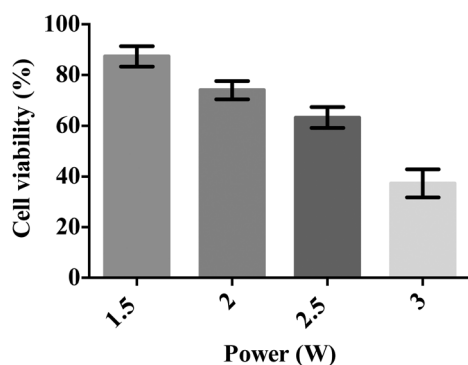


**Fig. 4** Post-nebulisation MSC viability as a function of the power applied to the SAW device, measured immediately after nebulisation using a trypan blue assay. The data are represented in terms of a mean value ( $n = 3$ )  $\pm$  standard error.

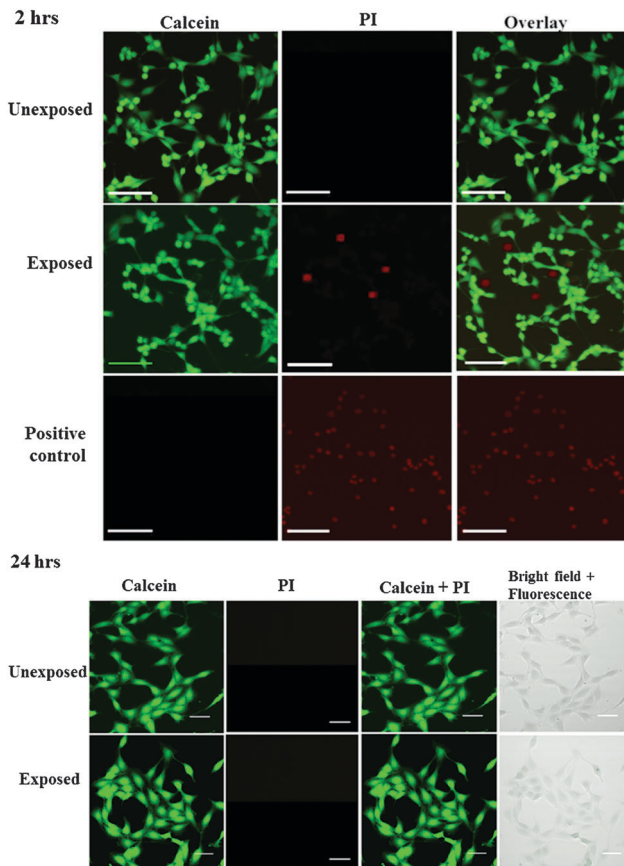


**Fig. 5** Viability of unexposed and nebulised MSCs, indicated by Calcein AM and PI staining. The cells were examined 2 h (top) and 24 h (bottom) post-nebulisation. Live cells stained by Calcein AM appear green and dead cells stained with PI appeared red. For the positive control, cells were treated with 0.1% Triton X-100 prior to staining. The scale bars represent a length of  $50 \mu\text{m}$ .

most of the MSCs were stained by Calcein AM (which appear in green), indicating that they remained viable after nebulisation. We observe these MSCs to have started to attach onto the well-plate. At 24 h post-nebulisation, it can be seen that the nebulised MSCs exhibited spindle-like morphologies similar to the untreated cells, indicating the retention of their structural integrity post-nebulisation. Furthermore, it can be seen that most of the cells were viable and were stained by Calcein AM. This was confirmed by the flow cytometry data wherein the representative dot plot of the Calcein AM intensity against the PI intensity in Fig. 6 shows that the majority of nebulised cells were stained with Calcein AM. Specifically, MSCs nebulised at 1.5 W exhibited a viability of  $86.0 \pm 4.2\%$  immediately after nebulisation. Nonetheless, it appeared that the growth of the MSCs recovered after re-culturing for another 24 h, at which we observe no significant difference in the cell viability between the nebulised MSCs and untreated MSCs ( $p = 0.026$ ,  $n = 4$ ), thus verifying that the SAW nebulisation does not lead to adverse effects on the MSC viability.

### Cell metabolic activity and proliferation

Nebulised MSCs were seeded in a well-plate and cultured over a period of 7 days to assess their metabolic activity and

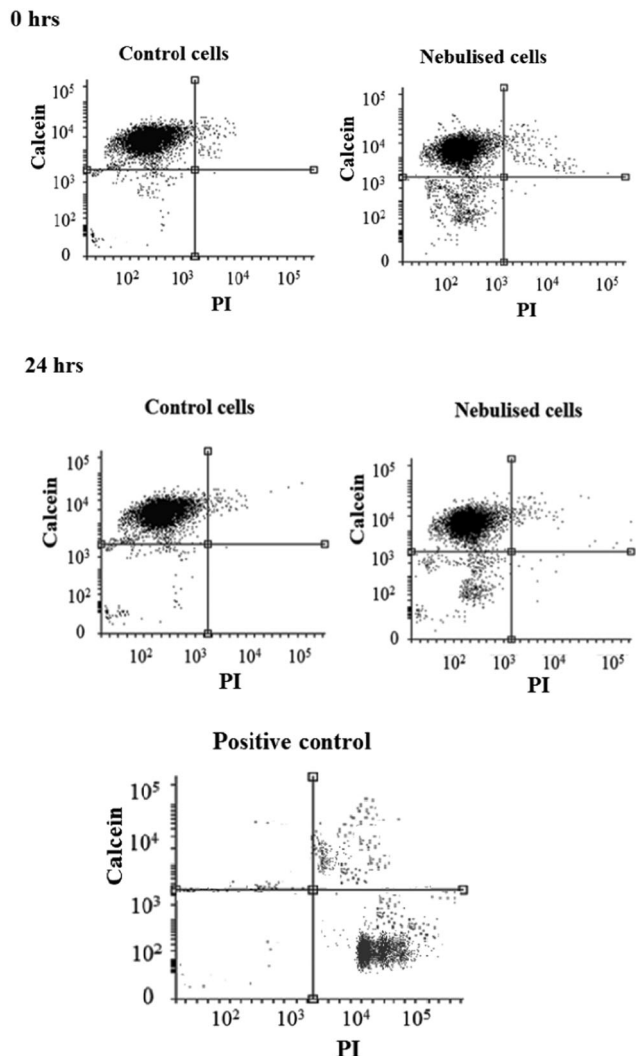


Fig. 6 Flow cytometry analysis indicating the viability in the population of unexposed and nebulised MSCs stained with Calcein AM and PI immediately after nebulisation and at 24 h after nebulisation. For positive control, cells were treated with 0.1% Triton X-100 prior to staining.

proliferation ability at different time points compared to the untreated cells (control). As shown in the representative optical microscopy images in Fig. 7, both nebulised and untreated MSCs expanded and occupied more of the substrate area over time. In addition, we find that the morphology of nebulised MSCs remains similar to that of the untreated MSCs.

To quantify the metabolic activity of nebulised cells, we carried out an AlamarBlue<sup>®</sup> assay wherein the cellular metabolic activity results in the chemical reduction of AlamarBlue<sup>®</sup>, manifesting as a measurable colour change in the redox indicator in the assay;<sup>38</sup> an increase in the amount of reduced AlamarBlue<sup>®</sup> is therefore an indication of an increase in metabolic activity. Fig. 8 shows the metabolic activity of the nebulised MSCs over a period of 7 days, calculated by normalising the extent of AlamarBlue<sup>®</sup> reduced by the nebulised cells compared to that reduced by the untreated cells. It can be seen that the metabolic activity of the nebulised MSCs increased over time, regardless of the power at which the

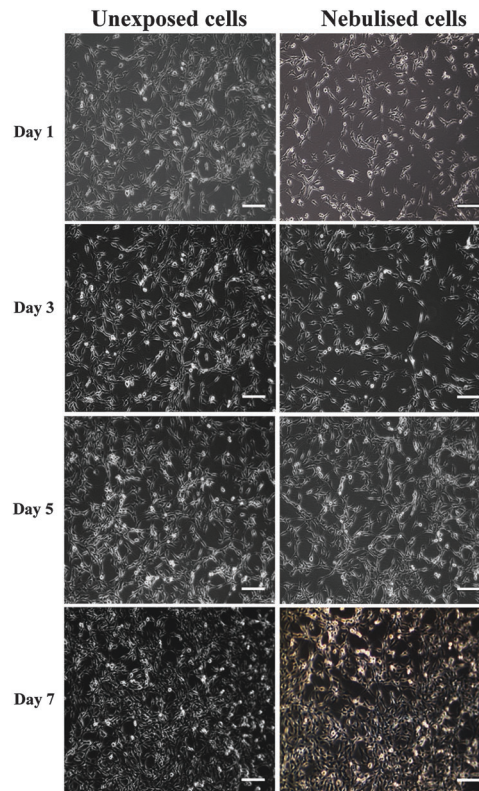


Fig. 7 Phase contrast images of unexposed (left column) and nebulised (right column) MSCs acquired at different incubation times. The majority of cells exhibited a spindle-like morphology. Scale bars represent a length of 100  $\mu\text{m}$ .

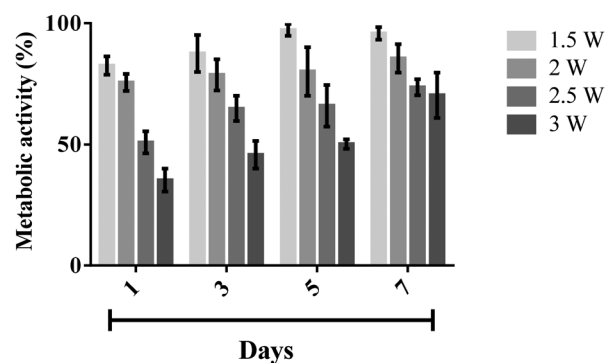


Fig. 8 Metabolic activity of nebulised MSCs at day 1, 3, 5, and 7, determined using an AlamarBlue<sup>®</sup> assay, the results of which were normalised against the activity of the control, *i.e.*, the unexposed cells (100% activity). The data are represented in terms of a mean value ( $n = 3$ )  $\pm$  standard error.

cells were nebulised, although we note that the metabolic activity of MSCs nebulised at 1.5 W was found to be the highest amongst the range of applied powers that were tested. This observation is however not surprising, given the decrease in cell viability with increasing power (Fig. 4) which is expected to influence the metabolic rate proportionally.

The strong correlation between the number of cells and DNA content allows us to determine the cellular proliferation rate with high accuracy. This was carried out by measuring the DNA

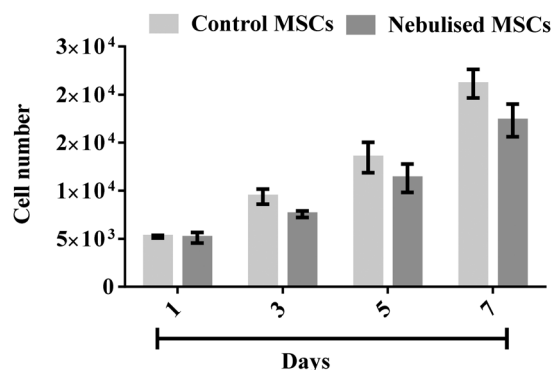


Fig. 9 MSC proliferation after nebulisation at 1.5 W. The cell proliferation was determined by quantifying the DNA content using a Quant-iT PicoGreen<sup>®</sup> dsDNA assay. The data are represented in terms of a mean value ( $n = 3$ )  $\pm$  standard error.

content of the MSCs over time using a Quant-iT PicoGreen<sup>®</sup> dsDNA assay. Fig. 9 shows that the number of MSCs from both the nebulised ( $p < 0.0001$ ,  $n = 3$ ) and untreated ( $p < 0.0001$ ,  $n = 3$ ) samples gradually increased over a 7 day period. We note that though the nebulised cells proliferated slightly slower from day 5 ( $p = 0.16$ ,  $n = 3$ ), nonetheless, the nebulised cells were observed to maintain their proliferation ability throughout the entire test duration.

### Gene and protein expression

MSCs possess multi-lineage potential to differentiate into a number of cell types including osteocytes, adipocytes and chondrocytes. They are known to express surface markers CD29, CD44, and CD106 positively, with these markers often being considered indicators for MSC isolation as well as differentiation,<sup>39–42</sup>

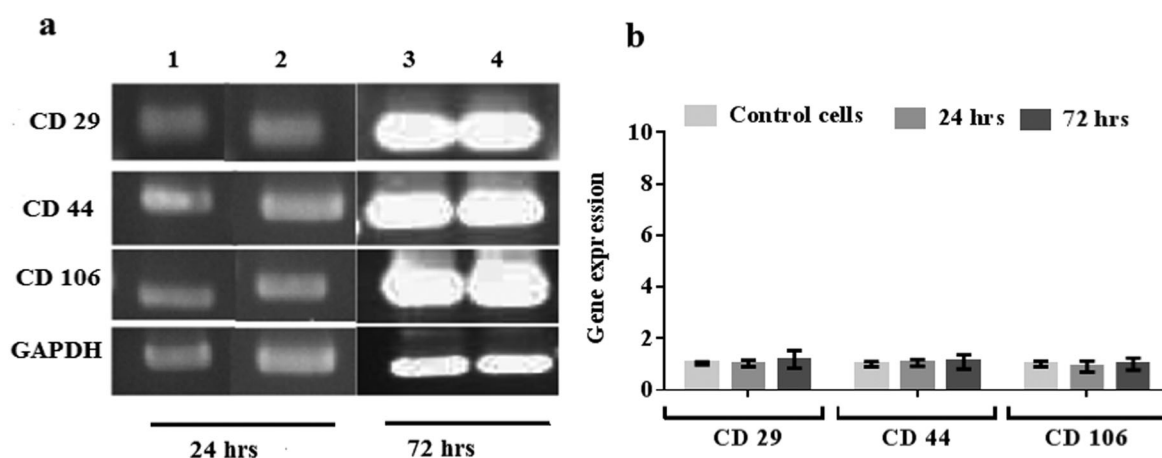


Fig. 10 (a) RT-PCR and (b) qPCR analysis of nebulised MSCs, showing the insignificant fold change in the gene expression relative to unexposed MSCs after 24 and 72 h. The error bars indicate the standard deviation of values acquired across the triplicate ( $n = 3$ ) data. In (a), lanes 1 and 3 represent the data for the unexposed cells (control) whereas lanes 2 and 4 represent those of the nebulised cells.

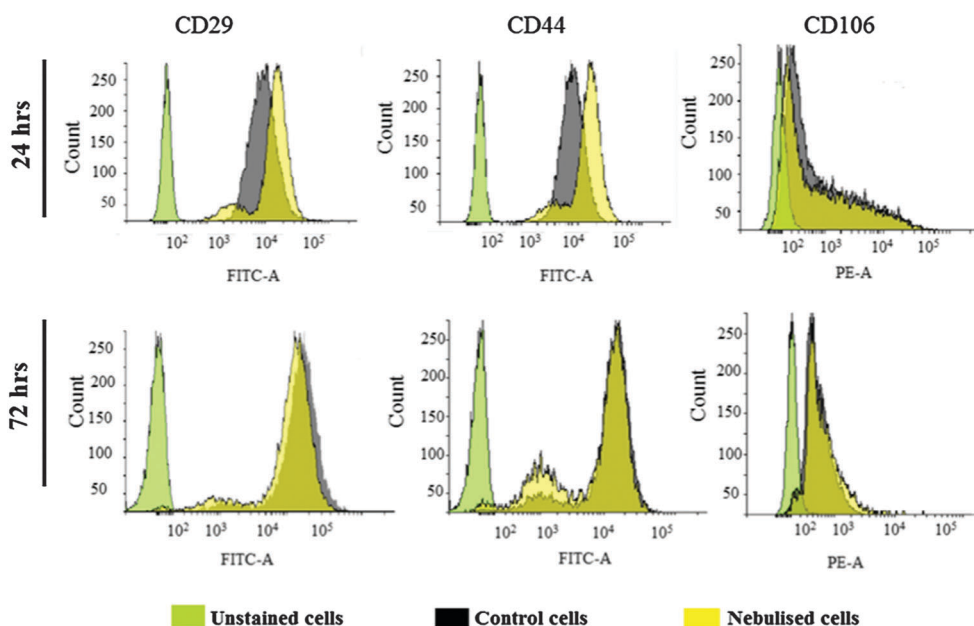


Fig. 11 Immunophenotypic profile of unexposed (control) and nebulised MSCs after incubation periods of 24 and 72 h.

and therefore used to assess the pluripotent phenotype and integrity of the MSCs prior to and after nebulisation at different time points. Fig. 10a shows the results from the RT-PCR analysis of the control and nebulised MSCs at 24 and 72 h wherein we observe both to express these markers, revealing that the nebulised cells are phenotypically similar to the control cells. The gene expression of the nebulised MSCs was further quantified using qPCR at different time points as shown in Fig. 10b. Compared to the control, the nebulised MSCs continued to express similar levels of CD29, CD44 and CD106 after 24 h ( $p = 0.92$ ,  $n = 4$ ;  $p = 0.6$ ,  $n = 4$  and  $p = 0.49$ ,  $n = 4$ , respectively) and 72 h ( $p = 0.5$ ,  $n = 4$ ;  $p = 0.65$ ,  $n = 4$ ;  $p = 0.98$ ,  $n = 4$ , respectively), suggesting that the SAW nebulisation did not lead to any alteration in the gene expression of the MSCs.

This is further verified from the results of the flow cytometry analysis employed to determine the protein expression of cells in Fig. 11, which shows the nebulised MSCs having similar CD29, CD44 and CD106 positive cell counts compared to the control after 24 h ( $p = 0.30$ ,  $n = 3$ ;  $p = 0.69$ ,  $n = 3$  and  $p = 0.16$ ,  $n = 3$ , respectively) and 72 h ( $p = 0.72$ ,  $n = 3$ ;  $p = 0.32$ ,  $n = 3$  and  $p = 0.83$ ,  $n = 3$ , respectively). Taken together, the results above therefore confirm that the SAW nebulisation does not cause any detrimental effect to the phenotype and integrity of the MSCs even after taking into account the longer culture period post-nebulisation, thus further verifying the SAW device as a promising platform for stem cell nebulisation.

## Conclusions

This study demonstrates the feasibility of generating MSC-laden aerosols using a SAW nebulisation platform without any deleterious effects on the cells. We found that an optimum power level of 1.5 W yielded a balance between maximising cell viability at an acceptable level of approximately 90% (measured after re-culturing for 24 h) whilst maintaining a practically useable delivery rate of  $100 \mu\text{L min}^{-1}$  for inhalation. This is verified by post-nebulisation assessment of the structure, metabolic activity, proliferation and genetic makeup of the MSCs, which indicate that the SAW nebulisation process does not lead to any significant adverse effects on the cell metabolic rate, proliferation ability, and genotypic and phenotypic characteristics compared to their non-nebulised counterpart. Given the novelty of inhaled stem cell therapy, comparisons with other delivery methods are difficult at present, although we anticipate that more data for benchmarking will become available in the literature in the near future with the increasing interest in stem cell therapy given the absence of viable alternative treatment regimes for respiratory ailments to date. Nonetheless, the results in this work provide compelling evidence that the SAW nebulisation platform, with its inherent benefits such as low cost and portability, constitutes an attractive tool for the delivery of stem cells *via* inhalation for treatment and repair of lung functions.

## Acknowledgements

Funding for this work was provided through Australia Research Council Discovery Grants DP120102570 and DP140100805. LA is grateful for a PhD scholarship from the Ministry of Higher Education & Scientific Research/Iraq. ARR is grateful for a RMIT University Vice-Chancellor's Research Fellowship. LYY gratefully acknowledges support from a Future Fellowship from the Australian Research Council under grant FT13010672. The authors acknowledge the help of Dr Dodie Pouniotis (School of Medical Sciences, RMIT University) with the analysis of the flow cytometry data.

## References

- 1 A. N. Lau, M. Goodwin, C. F. Kim and D. J. Weiss, *Mol. Ther.*, 2012, **20**, 1116–1130.
- 2 B. N. Gomperts and R. M. Strieter, *Annu. Rev. Med.*, 2007, **58**, 285–298.
- 3 S. S. Iyer and M. Rojas, *Expert Opin. Biol. Ther.*, 2008, **8**, 569–581.
- 4 D. J. Weiss, J. K. Kolls, L. A. Ortiz, A. Panoskaltis-Mortari and D. J. Prockop, *Proc. Am. Thorac. Soc.*, 2008, **5**, 637–667.
- 5 L. Y. Yeo, J. R. Friend, M. P. McIntosh, E. N. T. Meeusen and D. A. V. Morton, *Expert Opin. Drug Delivery*, 2010, **7**, 663–679.
- 6 K. M. G. Taylor and O. N. M. McCallion, *Int. J. Pharm.*, 1997, **153**, 93–104.
- 7 C. Harvey, M. O'Doherty, C. Page, S. Thomas, T. Nunan and D. Treacher, *Eur. Respir. J.*, 1997, **10**, 905–909.
- 8 D. I. Braghirolli, F. Zamboni, P. C. Chagastelles, D. J. Moura, J. Saffi, J. A. P. Henriques, D. A. Pilger and P. Pranke, *Biomicrofluidics*, 2013, **7**, 044130.
- 9 A. Abeyewickreme, A. Kwok, J. R. McEwan and S. N. Jayasinghe, *Integr. Biol.*, 2009, **1**, 260–266.
- 10 S. Sahoo, W. C. Lee, J. C. H. Goh and S. L. Toh, *Biotechnol. Bioeng.*, 2010, **106**, 690–698.
- 11 C. Ye, Z. He, Y. Lin, Y. Zhang, J. Tang, B. Sun, M. Ma, J. Liu, L. Yang, H. Ren and B. Zhao, *Biotechnol. Lett.*, 2015, **37**, 449–456.
- 12 L. Y. Yeo and J. R. Friend, *Annu. Rev. Fluid Mech.*, 2014, **46**, 379–406.
- 13 X. Ding, P. Li, S.-C. S. Lin, Z. S. Stratton, N. Nama, F. Guo, D. Slotcavage, X. Mao, J. Shi, F. Costanzo and T. J. Huang, *Lab Chip*, 2013, **13**, 3626–3649.
- 14 M. Kurosawa, T. Watanabe, A. Futami and T. Higuchi, *Sens. Actuators, A*, 1995, **50**, 69–74.
- 15 M. P. Flament, P. Leterme and A. Gayot, *Drug Dev. Ind. Pharm.*, 2001, **27**, 643–649.
- 16 A. Qi, L. Yeo, J. Friend and J. Ho, *Lab Chip*, 2010, **10**, 470–476.
- 17 F. Guo, P. Li, J. B. French, Z. Mao, H. Zhao, S. Li, N. Nama, J. R. Fick, S. J. Benkovic and T. J. Huang, *Proc. Natl. Acad. Sci. U. S. A.*, 2015, **112**, 43–48.
- 18 A. Qi, J. R. Friend, L. Y. Yeo, D. A. V. Morton, M. P. McIntosh and L. Spiccia, *Lab Chip*, 2009, **9**, 2184–2193.
- 19 C. Cortez-Jugo, A. Qi, A. Rajapaksa, J. R. Friend and L. Y. Yeo, *Biomicrofluidics*, 2015, **9**, 052603.

- 20 A. Rajapaksa, J. Ho, A. Qi, T.-H. Nguyen, M. Tate, R. Bischof, D. Piedrafta, M. McIntosh, L. Yeo, E. Meeusen, R. Coppel and J. Friend, *Respir. Res.*, 2014, **15**, 60.
- 21 J. Ho, M. K. Tan, D. B. Go, L. Y. Yeo, J. R. Friend and H.-C. Chang, *Anal. Chem.*, 2011, **83**, 3260–3266.
- 22 S. R. Heron, R. Wilson, S. A. Shaffer, D. R. Goodlett and J. M. Cooper, *Anal. Chem.*, 2010, **82**, 3985–3989.
- 23 Y. Huang, S. Yoon, S. Heron, C. Masselon, J. S. Edgar, F. Tureček and D. Goodlett, *J. Am. Soc. Mass Spectrom.*, 2012, **23**, 1062–1070.
- 24 M. Alvarez, J. R. Friend and L. Y. Yeo, *Langmuir*, 2008, **24**, 10629–10632.
- 25 H. Li, J. Friend, L. Yeo, A. Dasvarma and K. Traianedes, *Biomicrofluidics*, 2009, **3**, 034102.
- 26 N. R. Glass, R. J. Shilton, P. P. Y. Chan, J. R. Friend and L. Y. Yeo, *Small*, 2012, **8**, 1881–1888.
- 27 A. Qi, P. Chan, J. Ho, A. Rajapaksa, J. Friend and L. Yeo, *ACS Nano*, 2011, **5**, 9583–9591.
- 28 R. Shilton, M. K. Tan, L. Y. Yeo and J. R. Friend, *J. Appl. Phys.*, 2008, **104**, 014910.
- 29 S. P. Hoo, F. Sarvi, W. H. Li, P. P. Y. Chan and Z. Yue, *ACS Appl. Mater. Interfaces*, 2013, **5**, 5592–5600.
- 30 F. Sarvi, K. Jain, T. Arbatan, P. J. Verma, K. Hourigan, M. C. Thompson, W. Shen and P. Chan, *Adv. Healthcare Mater.*, 2015, **4**, 77–86.
- 31 A. Ode, A. Kurtz, K. Schmidt-Bleek, P. Schrade, P. Kolar, F. Buttgerit, K. Lehmann, D. Hutmacher, G. Duda and G. Kasper, *Eur. Cells Mater.*, 2011, **22**, 26–42.
- 32 H. Qin, L.-D. Zhao, J.-H. Sun, L.-L. Ren, W.-W. Guo, H.-Z. Liu, S.-Q. Zhai and S.-M. Yang, *Acta Oto-Laryngol.*, 2011, **131**, 1136–1141.
- 33 H. Y. Lau and M. Bhatia, *Am. J. Physiol.: Gastrointest. Liver Physiol.*, 2007, **292**, G1283–G1292.
- 34 S. Schäfer, A.-G. Calas, M. Vergouts and E. Hermans, *J. Neuroimmunol.*, 2012, **249**, 40–48.
- 35 J. C. Sung, B. L. Pulliam and D. A. Edwards, *Trends Biotechnol.*, 2007, **25**, 563–570.
- 36 J. Heyder, J. Gebhart, G. Rudolf, C. F. Schiller and W. Stahlhofen, *J. Aerosol Sci.*, 1986, **17**, 811–825.
- 37 H. Li, J. Friend, L. Yeo, A. Dasvarma and K. Traianedes, *Biomicrofluidics*, 2009, **3**, 034102.
- 38 G. K. Das, P. P. Y. Chan, A. Teo, J. S. C. Loo, J. M. Anderson and T. T. Y. Tan, *J. Biomed. Mater. Res., Part A*, 2010, **93**, 337–346.
- 39 L. d. S. Meirelles and N. B. Nardi, *Br. J. Haematol.*, 2003, **123**, 702–711.
- 40 M. F. Pittenger, A. M. Mackay, S. C. Beck, R. K. Jaiswal, R. Douglas, J. D. Mosca, M. A. Moorman, D. W. Simonetti, S. Craig and D. R. Marshak, *Science*, 1999, **284**, 143–147.
- 41 Y. A. Romanov, A. N. Darevskaya, N. V. Merzlikina and L. B. Buravkova, *Bull. Exp. Biol. Med.*, 2005, **140**, 138–143.
- 42 D. A. De Ugarte, K. Morizono, A. Elbarbary, Z. Alfonso, P. A. Zuk, M. Zhu, J. L. Dragoo, P. Ashjian, B. Thomas, P. Benhaim, I. Chen, J. Fraser and M. H. Hedrick, *Cells Tissues Organs*, 2003, **174**, 101–109.